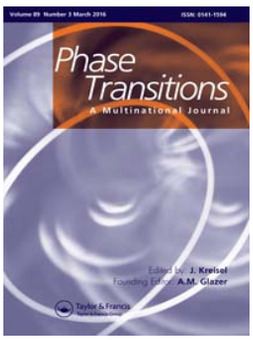

Taylor & Francis
Taylor & Francis Group

Phase Transitions
A Multinational Journal

ISSN: 0141-1594 (Print) 1029-0338 (Online) Journal homepage: https://www.tandfonline.com/loi/gpht20

Effect of cobalt doping on structural, optical and redox properties cerium oxide nanoparticles

Anees A. Ansari, J. Labis, M. Alam, Shahid M. Ramay, N. Ahmad & Asif Mahmood

To cite this article: Anees A. Ansari, J. Labis, M. Alam, Shahid M. Ramay, N. Ahmad & Asif Mahmood (2016) Effect of cobalt doping on structural, optical and redox properties cerium oxide nanoparticles, Phase Transitions, 89:3, 261-272, DOI: 10.1080/01411594.2015.1116532

To link to this article: https://doi.org/10.1080/01411594.2015.1116532

Phase Transitions, 2016
Vol. 89, No. 3, 261–272, http://dx.doi.org/10.1080/01411594.2015.1116532

Effect of cobalt doping on structural, optical and redox properties cerium oxide nanoparticles

Anees A. Ansari [a]*, J. Labis[a], M. Alam[b], Shahid M. Ramay[c], N. Ahmad[b] and Asif Mahmood[d]

[a]*King Abdullah Institute for Nanotechnology, King Saud University, Riyadh, Saudi Arabia;* [b]*Research Center, College of Sciences, King Saud University, Riyadh, Saudi Arabia;* [c]*Department of Physics, King Saud University, Riyadh, Saudi Arabia;* [d]*Department of Chemical Engineering, College of Engineering, King Saud University, Riyadh, Saudi Arabia*

(*Received 13 May 2015; accepted 2 November 2015*)

Cobalt-doped ceria nanoparticles were synthesized using the polyol method under co-precipitation hydrolysis. The structural, morphological, optical and redox properties were observed to investigate the influence of different concentration of cobalt ion doping on the prepared CeO_2 nanomaterials in terms of X-ray diffraction, field-emission transmission electron microscopy, thermogravimetric analysis, Fourier-transform infrared spectroscopy, UV/vis absorption spectroscopy and temperature program reduction techniques. The optical band gap energy was calculated from the optical absorption spectra for doped ceria nanoparticles, which have been found to be 2.68, 2.77, and 2.82 eV for the 2, 4, and 7 mol% Co ion-doped CeO_2 nanoparticles, respectively. As observed, the band gap energies increases as the doping Co ion concentrations increased, which could be due to significant increased oxygen vacancies with Co doping. The synergistic interaction between Co and CeO_2 was the main factor responsible for high catalytic activity of cobalt-doped CeO_2 model catalysts.

Keywords: structural ceramic materials; chemical synthesis; X-ray diffraction; redox properties

1. Introduction

In recent years, research interest on CeO_2 and doped CeO_2 nanoparticles are increasing, due to that possession, many attractive properties make them highly promising materials for diverse applications, such as solid electrolytes or anode materials in solid oxide fuel cells, automotive three-way catalysts, a water-gas shift catalyst, ultraviolet absorbers, oxygen sensors, and catalysts for dehydrogenation of higher alcohols.[1–10] However, the most relevant use of CeO_2-based compounds is in automotive pollution control, as promoters of the so-called three-way catalyst.[1,6] Almost all vehicles nowadays are equipped with catalytic converters, which invariably contain some CeO_2-containing oxide as catalyst promoter. The wide use of these systems as catalyst components promoted renewed interest with regards to these materials in the form of nano-sized, high surface area powders. The possibility of producing redox nanomaterials with tunable redox capability to activate simple reactants has recently been explored.[1,3–5] Nano-structured materials which provide novel properties appear to be a cutting edge frontier in designing catalysts and catalyst promoters for specific catalytic reactions.[3–8]

*Corresponding author. Email: amustaqeemahmad@ksu.edu.sa

Nowadays, it has been a continuous search for metal ions doping that promote the ionic conductivity of CeO_2 nanoparticles at moderate temperature. A range of potential dopant materials has been employed to promote the ionic conductivity of the synthesized CeO_2 nanopowder.[1−5] Radovic et al. employed the hydrothermal method for the preparation of iron-doped CeO_2 nanoparticles to investigate the effect of iron doping on optical properties of nanomaterial.[11] Some researchers have shown that iron-containing nanocrystalline CeO_2 is an active and stable catalyst in low- and high-temperature redox reactions.[12,13] Copper-doped ceria has been employed to enhance the catalytic activity over the wide range of temperature.[14] Some rare earth metal ions have been doped in CeO_2 lattice to enhance the ionic conductivity of the materials and investigate their applications for solid oxide fuel cells.[3,4,15] Fu et al. doped low contents of Au in CeO_2 nanoparticles to enhance the catalytic activity of the materials.[16] Some other groups have synthesized noble metal-supported CeO_2 for their applications in the three-way automotive catalyst that enhance low-temperature water gas shift reaction.[5,17] The reducibility and catalytic activity of CeO_2 was significantly enhanced by the presence of a small amount of transition metals, outside the platinum group. Platinum was the first metal demonstrated to have a considerable effect on CeO_2 reducibility.[5] However, the cost of noble metal ions are high and is the main drawback for their use in developing catalytic materials. In this study, we considered cobalt ion as an ionic conductivity promoter because it is the neighborhood of the above-mentioned two elements. Moreover, based on the effect of severely under sized dopant ions reported by Chen and Chen [18], the Co^{2+} ion may have the tendency to enhance grain boundary mobility of CeO_2, since its ionic size is much smaller than that of the matrix ion (i.e. Ce^{4+}). To our knowledge, there are only a very few literature reports concerning the redox behavior of CeO_2 with Co as an additive.[19−21] Furthermore, Co was reported as an effective dopant for the densification of SnO_2.[22,23] Varela et al.[22] and Cerri et al.[23] reported that the addition of 0.5−2 mol% CoO into SnO_2 promotes the densification of this oxide up to ∼99.0% of the theoretical density; and the sintering of Co-doped SnO_2 seems to be controlled by solid state diffusion because of the absence of experimental evidence for an eutectic liquid in this system. They deduced that Co^{2+} ions incorporating into SnO_2 crystallites have acted as an acceptor leading to the addition of oxygen vacancies into SnO_2, thus enhancing the densification rate of this oxide.

In this paper, we report the synthesis of different concentrations of Co-doped CeO_2 nanoparticles by the complexing hydrothermal co-precipitation method. The synthesized doped CeO_2 nanoparticles were analyzed by X-ray diffraction (XRD), thermogravimetric analysis (TGA), field-emission transmission electron microscopy (FE-TEM), energy dispersive X-ray analysis (EDX), UV/vis absorption spectra, optical band gap energy, Fourier transform infrared (FTIR) spectroscopy and temperature-programmed reduction (TPR) measurements. In addition, the morphological structure, optical properties, and thermal stability of the synthesized nanophosphors were also systematically studied in this article.

2. Experimental

2.1. Materials and methods

Cerium nitrate (99.99%, BDH Chemicals Ltd, England), cobalt nitrate (E-Merck, Germany) ethylene glycol, C_2H_5OH, and NH_4OH were used as starting materials without

any further purification. The ultrapure deionized water was used for the preparation of solutions. The ultrapure deionized water was prepared using a Milli-Q system (Millipore, Bedford, MA, USA). All other chemicals used were of reagent grade.

2.2. Preparation of Co ion-doped cerium oxide nanoparticles

In a typical reaction, 0.2M $Ce(NO_3)_3$ $6H_2O$ (0.98, 0.96, and 0.93 mol%) was dissolved in 50 ml ethylene glycol and heated on a hot plate upto 80 °C. Separately, 0.02M cobalt nitrate (0.02, 0.04, and 0.07 mol%) dissolved in ethylene glycol was added drop-wise in the foregoing reaction and the whole solution mixture was kept on a hot plate with magnetic stirring at 80 °C to obtain a homogenous mixture. Later, homogenously mixed solution was transferred in a 250 ml flask fitted with reflux condenser and hydrolyzed for 24 h. An amount of ammonia was added to the hydrolyzed solution and the precipitate was obtained. The obtained gray-colored precipitate was centrifuged and washed several times with distilled water to remove the excess amount of ammonium and nitrate ions, the obtained product was dried at 100 °C. The prepared samples were annealed at 400 °C in air for 2 h. We examined the systematic changes in the color of the cerium hydroxide precipitate. The color of the prepared cerium hydroxide precipitate was changed gradually from gray to yellow after being exposed to air. This may be due to the oxidation of peroxide Ce $(OH)_3OOH$ to $Ce(OH)_4$ by oxygen. This procedure was repeated for synthesis and purification of different Co-doped CeO_2 concentrations.

2.3. Characterization

The crystalinity of the powder samples were examined by XRD at room temperature with the use of Rigaku-Dmax 2500 diffractometer equipped with Cu K_α (λ = 1.54056 Å) radiations as the X-ray source. TGA was performed with TGA/DTA, Mettler Toledo AG, Analytical CH-8603, Schwerzenbach, Switzerland. The size and morphology of the samples were inspected using a FE-TEM equipped with the EDX (FETEM, JEM-2100F, JEOL, Japan) operated at an accelerating voltage of 200 kV. EDX analysis was used to confirm the presence of the elements. The samples for TEM were prepared by depositing a drop of the colloidal ethanol solution of the powder sample onto a carbon-coated copper grid. The FTIR spectra were recorded on a Perkin-Elmer 580B IR spectrometer using a KBr pellet technique in the range 4000−400 cm^{-1}. The UV/vis absorption spectra were measured in the Perkin-Elmer Lambda-40 spectrophotometer in the range 200−600 nm, with the sample contained in 1 cm^3 stoppered quartz cell of 1 cm path length. TPR by H_2 (H_2-TPR) was performed with the Thermo-Finnigan TPDRO 1100 instrument with a thermal conductivity detector. Before detection, the gas was purified by a solid trap containing CaO + NaOH materials in order to remove the H_2O and CO_2. The quartz tube reactor was loaded with 50 mg sample in powder form and heated from room temperature to 900 °C in 5% H_2/N_2 mixture with a flow rate of 20 ml min^{-1}. By replacing the 5% H_2/N_2 with 5% CO/He, the CO-TPR tests were also carried out. After the sample was reduced by 5% H_2/N_2 from room temperature to 500 °C and held for 10 min, temperature-programmed oxidation tests were performed from room temperature into 900 °C in 6% O_2/He flow at a rate of 20 ml min^{-1}. All measurements were performed at room temperature.

3. Results and discussion

3.1. Crystallographic morphology

The crystal structure and phase purity of the Co-doped CeO_2 nanostructures in Figure 1 are analyzed by XRD. The principal reflections as seen in the diffraction patterns can be ascribed to fluorite CeO_2. All reflection peaks correspond to the (111), (200), (220), (311), and (222) planes, which are well indexed and identified to the pure CeO_2 nanoproduct (space group: *Fm*3*m*), has the cubic fluorite phase (JCPDS card 12-0797). [24–26] The broad and sharp reflection peaks suggest that the prepared products are well crystallized and very small in sizes. The intensities and positions of the diffraction peaks are in good agreement with the literature data. No Co_3O_4 and other salts can be observed by XRD over the entire doping range. The absence of impurity peaks indicates good incorporation of Co into the lattice sites of CeO_2 or the amount is too small to be detected by XRD. Furthermore, the structure of the as-generated Co-doped CeO_2 could have remained the same upon doping. This means the formation of homogeneous Co–Ce–O solid solutions.[27,28] The calculated lattice parameter for the as-prepared 2%, 4%, and 7% Co-doped CeO_2 products are found to be (1) 5.4089 Å, (2) 5.4086 Å, (3) 5.407 Å, respectively, which are slightly lower than its bulk counterpart (5.411 Å). The calculated average grain size as estimated from the Debye–Scherrer formula using the half width of diffraction peak of (111) plane, 15.4 nm for 2, 13.39 nm for 4, and 12.6 nm for 7 mol% Co-doped CeO_2. Yet, the gradual decrease in the peak intensity and the slight increase in the peak width with the introduction of Co indicate that the grain size is minimal after Co doped into CeO_2 lattice. On the other hand, the diffraction peaks of Co–Ce–O shift slightly to higher angle by comparison with pure sample, resulting from the CeO_2 lattice contraction and the generation of the lattice distortion in the doped nanoparticles, which is attributed to the substitution of the smaller divalent Co ion[$r(Co^{2+}) = 0.65$ nm] for Ce^{4+} [$r(Ce^{4+}) = 0.97$ nm].[27,29] It is observed that CeO_2 and Co-doped CeO_2 nanoparticles experience considerable lattice deformation, which is in good agreement with earlier reports.[27,19–21] Those reports indicated that doping caused a change in the Ce–O bond length (lattice distortion) and on the overall lattice parameter.[29–33]

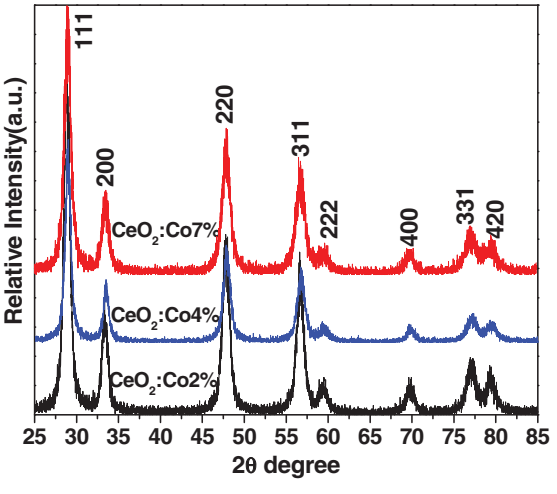

Figure 1. X-ray diffraction pattern of cobalt-doped cerium oxide nanoparticles.

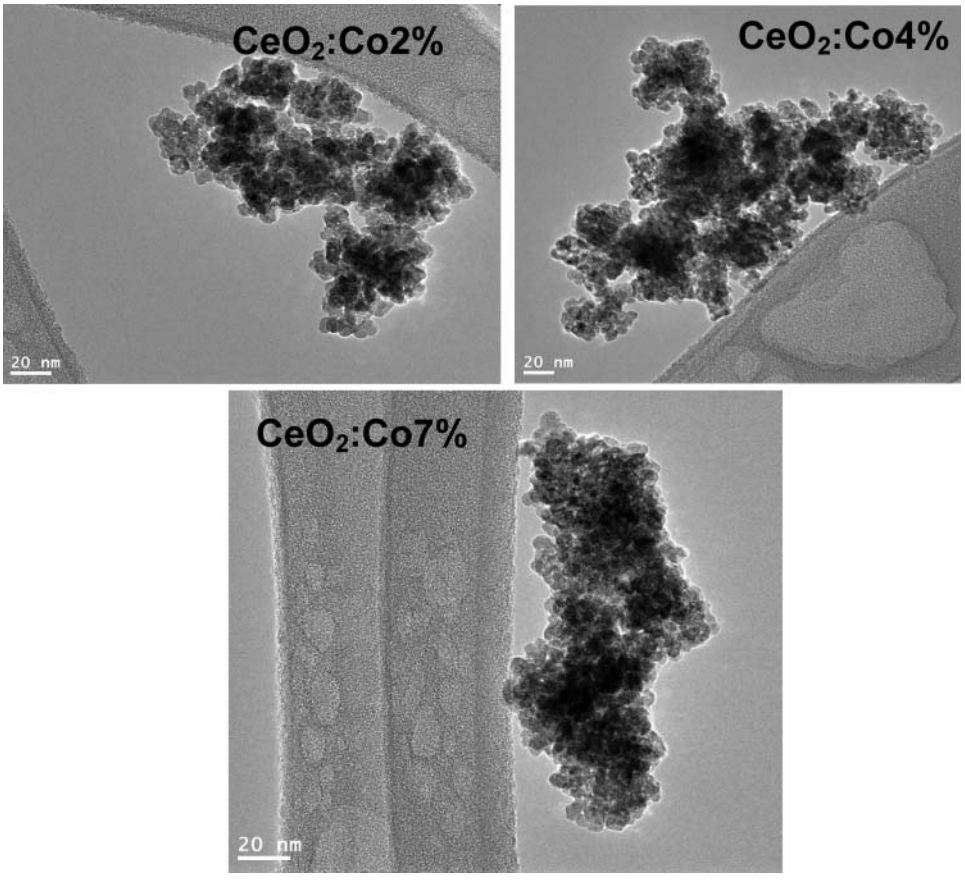

Figure 2. FE-TEM micrographs of cobalt-doped cerium oxide nanoparticles.

The size and morphology of the prepared Co-doped CeO_2 nanoparticles were analyzed by the TEM images. Figure 2 clearly shows the typical image of Co-doped CeO_2 nanoparticles. TEM image reveals that hydrothermal-co-precipitated nanoproducts consist of well crystalline and highly agglomerated nanoparticles in spherical morphology with sizes ranging from 12.6 to 15.4 nm. The results were in good agreement with the XRD data. EDX analysis confirmed the formation of single-phase Co-doped CeO_2 nanoparticles (Figure 3). The presence of Co in the 2%, 4%, and 7% Co-doped CeO_2 nanoparticles was indicated by the EDX spectrum. No Co phase was detected by the XRD, confirming that Co was doped into the CeO_2 lattice. An increase in the Co dopant concentration enhances the presence of Co (weight %) as confirmed by the EDX spectrum.

3.2. Thermogravimetric analysis

TGA was performed to determine the thermal stability and desorption temperature of various species between the temperature range of ~25 °C−800 °C under nitrogen atmosphere at a heating rate of 10 °C/min (Figure 4). The thermograms of Co-doped CeO_2 nanoparticles are all similar in shape and show degradation of their constituents into two decomposition steps. There is a ~2%–3.5% weight loss upto 200 °C (Figure 4(a) and

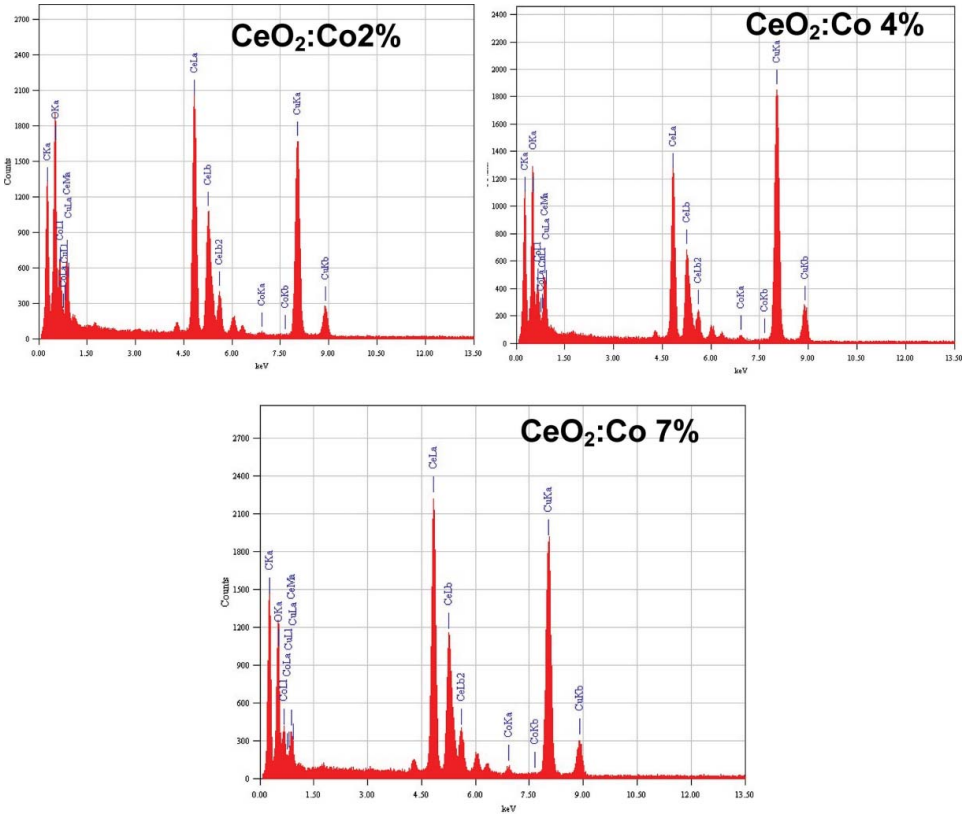

Figure 3. EDX analysis of the as-prepared cobalt-doped cerium oxide nanoparticles.

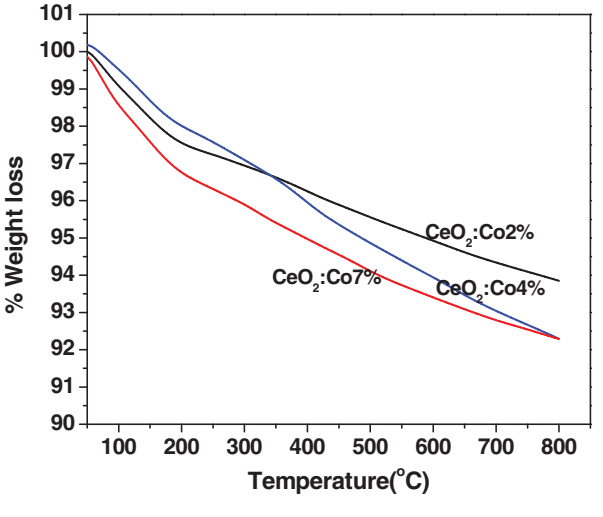

Figure 4. Thermo-gravimetric analysis of cobalt-doped cerium oxide nanoparticles.

4(b)), whereas nanoparticles (Figure 4(c)) shows 3.5% weight loss. This is slightly higher than that of Figure 4(a) and 4(b) doped nanoparticles. It mainly resulted from the removal of chemisorbed water and the release of organic residues that are trapped inside the pores. The second stage decomposition is observed between 200 °C and 800 °C (weight loss 4%−4.5%), which is likely due to the burning and elimination of surface OH groups. It is known that there are two types of surface OH groups, terminal Ce−OH and bridge Ce−(OH)–Ce.[34] Dissociation temperature of these surface OH groups differs from each other depending upon the chemical surroundings. Thus, the decrease in weight occurs in a rather wide range of temperature. No peaks corresponding to further crystallization are found on the DTA curve, indicating that the samples are crystalline. This is further confirmed by XRD. After heating at 800 °C, no obvious weight loss is observed.

3.3. Optical properties

Figure 5 shows the FTIR spectra of prepared Co-doped CeO_2 nanoparticles. An infrared broad band along with weak intensity bands located at ∼3433, 1623, 1331, and 1066 cm^{-1} are observed, which can be ascribed to ν(O−H) stretching vibration and δ(OH) bending vibrations, respectively, of the physically adsorbed water molecules on the nanoparticle surface (Figure 5(a)−5(c)).[34,35] The residual water or hydroxyl groups are also detected from the TGA analysis. An intense band located at around 500–400 cm^{-1} is attributed to Ce−O stretching vibration modes and thus reveal the formation of the Ce−O−Co network within the nanoparticles.[35]

Figure 6 shows the optical absorption spectra of the Co-doped CeO_2 nanoparticles. A strong absorption band emerges at the UV range of 270−400 nm, which originate from the charge transfer between the O^{2-} 2p and Ce 4f states.[34−36] The spectral profile indicates a charge-transfer transition of Ce^{4+} overlaps with the $4f^1 \rightarrow 5d^1$ transition of Ce^{3+}. No absorption is detected above 500 nm in wavelength. It is evident from the spectra that the adsorption edge shifted toward longer wavelength (red-shift) with increasing Co-dopant concentration that is contrast with the bulk CeO_2 powder data.

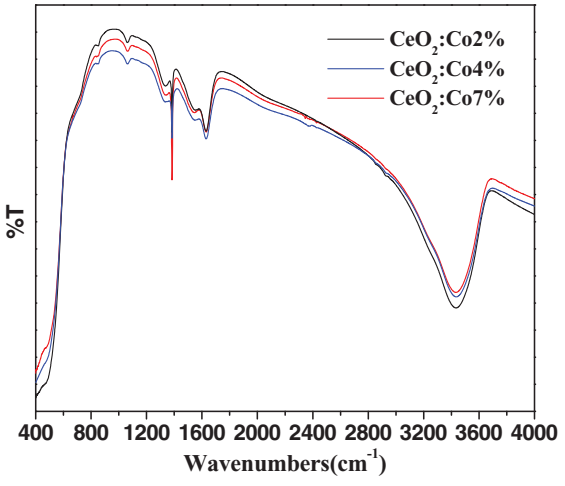

Figure 5. FTIR spectra of cobalt-doped cerium oxide nanoparticles.

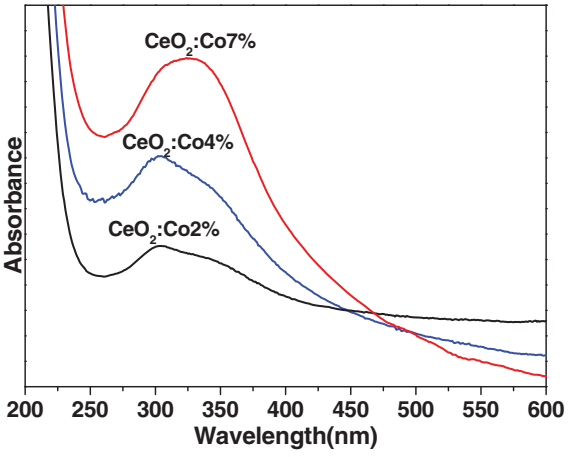

Figure 6. UV/vis absorption spectra of cobalt-doped cerium oxide nanoparticles suspended in ethanol.

The plots of $(\alpha h\nu)^2$ vs. photon energy of different Co ion-doped CeO_2 nanoparticles are shown in Figure 7. The optical band gap value can be determined by fitting the absorption data to the direct transition equation by extrapolating the linear portions of the curves to zero absorption

$$\alpha h\,\nu = E_D(h\nu - E_g)^{1/2},$$

where α is the optical absorption coefficient, $h\nu$ is the photon energy, E_g is the direct band gap, and E_D is a constant.[28,36] The correlated band gap energies are 2.68, 2.77, and 2.82 eV for the 2, 4, and 7 mol% Co ion-doped CeO_2 nanoparticles, respectively. Figure 7 shows that an increase in the dopant concentration results in an increase of the optical band gap energy. The lowest band gap value is seen in the case of the 2 mol% Co-doped CeO_2 nanoparticles. The reason for the enhanced performance in the case of doped CeO_2 is due to the fact that the addition of Co ions results in the formation of interstitial

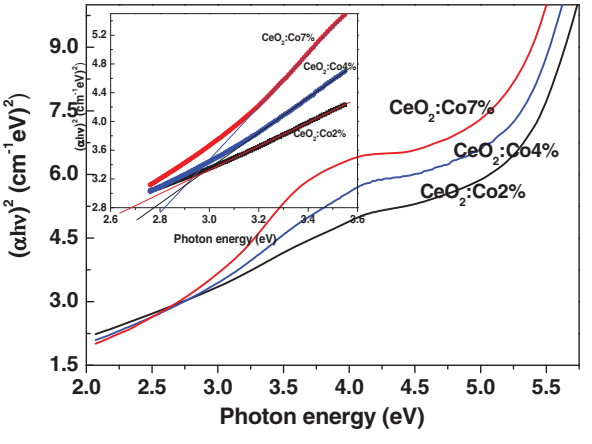

Figure 7. The plot of $(\alpha h\upsilon)^2$ vs. photon energy($h\upsilon$) of cobalt-doped cerium oxide nanoparticles.

sites, which in turn create new energy levels (impurity energy levels) between the valence and conduction bands.[28,36] The impurity energy levels allow for intrinsic band gap excitation under the visible light region. This implies that the higher energy state of 3d-electrons from Co-cation dopants can be excited to the conduction band of CeO_2,[37] thereby enhancing its catalytic performance. Similar values are within the range reported in the literature.[38] Saranya et al. observed Co-doped CeO_2 (2.84 eV) compared with that of pure CeO_2 (3.13 eV) nanoparticle.[39] Yue and Zhang reported that doping CeO_2 with Co could reduce the band gap of CeO_2 more effectively than do other transition-metal dopants.[40] Masui et al. reported the band gaps of 4.1 and 2.6 nm CeO_2 nanoparticle prepared using reverse micelles to be 3.38 and 3.44 eV, respectively.[41] Doping with Co ions creates oxygen vacancies and favors the formation of Ce^{3+} from Ce^{4+}. This increases the amount of Ce^{3+} states, resulting in the formation of localized energy states that are closer to the conduction band [42] thereby decreasing the band gap.

3.4. TPR studies

The H_2-TPR characterization is performed to investigate reducibility features of the as-prepared Co ion-doped CeO_2 catalysts, and the results are shown in Figure 8. In our experimental results, we observed two reduction peaks in pure CeO_2, one at about 122 °C and the other at 402 °C, which attributed to the reduction of surface capping oxygen and bulk oxygen species, respectively.[43] In our experimental case, the reduction temperatures are much lower than the reported temperature of ~500 °C and ~800 °C.[44] As the Co metal ion introduce into the CeO_2 lattice, the observed reduction peaks shift to lower temperature. It indicates that Co ion greatly promotes the surface reduction, as observed the sharp reduction peak at 305 °C in 2 mol% Co-doped CeO_2 nanoparticles, possibly due to the hydrogen spillover effect. Similarly, the degree of promotion increases as the doping concentrations of Co ion increases. Concerning the reduction pattern of CeO_2, two main reduction peaks can be observed, one at 112 °C and the other at 305 °C, due to the two-step reduction of Co_3O_4 involving CoO intermediate.[43] The second peak observed at 274 °C for the 7 mol% Co-doped CeO_2 is much lower as compared to pure CeO_2, which is at 403 °C. It assumes that this peak consumes much more H_2 for the

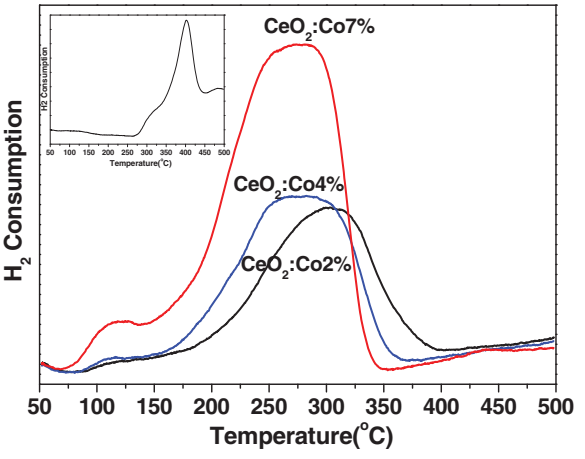

Figure 8. H_2-TPR profiles of cobalt-doped cerium oxide nanoparticles.

reduction on the Co-doped CeO_2 catalyst compared to pure CeO_2 nanoparticles. It clearly indicates that Co ions interact with the ceria nanoparticles within the surface lattice and these surface Co ions promote the reduction of the CeO_2 surface. However, the H_2 consumption of the 7 mol% Co-doped CeO_2 is lower than that of 4 mol% Co-doped CeO_2. This is probably because the dispersion of Co particles on the surface partly blocks the reduction of the ceria. The broad peak associated with the reduction of the bulk CeO_2 is significantly shifted for the 7 mol% Co-doped sample and the 4 mol% Co-doped sample. However, the peak area for three samples are different and show that the Co doping have significant influence on the reduction of bulk CeO_2. Comparing the relative intensity of the second peak for three samples, it is quite clear that the amount of reducible Co is higher in the 7 mol% Co-doped CeO_2 sample than in the 2 mol% Co-doped CeO_2 nanoparticles. It is obvious that the $Ce_{0.93}Co_{0.07}O_2$ nanoparticles show high redox properties at low temperature among Co-doped CeO_2 nanoparticles with various cobalt contents. As we know, CeO_2 can uptake and release oxygen via the transformation between Ce^{3+} and Ce^{4+}. As we discussed previously, after Co doping, the $Ce_{1-x}Co_xO_2$ solid solution might form partially. Therefore, Co-doped CeO_2 nanoparticles can easily uptake and release oxygen via the transition of Co^{2+}/Co^{3+} and Ce^{3+}/Ce^{4+}, and at the meantime, surface oxygen can participate in CO oxidation. So, beyond doubt, the catalytic redox activity of Co-doped CeO_2 nanoparticles is very important for the CO oxidation. Consequently, the $Ce_{0.93}Co_{0.07}O_2$ nanoparticles may exhibit an excellent catalytic performance at the lowest temperature as a result of the highest redox properties, which will also be confirmed by the catalytic activity evaluation.[45,46] This is further consistent with the EDX results showing that Co is distributed uniformly within the lattice of the Co-doped sample.

4. Conclusions

Nanocrystalline cobalt ion-doped CeO_2 particles with an average size 12.6−15.4 nm and narrow size distribution have been directly synthesized by a polyol-assisted co-precipitation process, which is confirmed by powder XRD, EDX, and optical absorption studies. It was found by XRD and optical absorption that an increase doping concentration of Co alters the crystalinity of the materials due to an increase in the oxygen vacancies inside the CeO_2 lattice. The band gap energies were also affected after increasing the doping contents of Co ion in CeO_2 lattice. TPR measurements revealed that enhanced doping concentration of Co ion enhanced redox properties and high doping content in CeO_2 promote to reduce at low temperature due to the doping effect. The simple preparation approach holds promises in the future large-scale synthesis of cobalt-doped CeO_2 nanoparticles for applications in solid electrolytes, electrochemical biosensor, and electrochromic devices.

Disclosure statement

No potential conflict of interest was reported by the authors.

Funding

The authors extend their sincere appreciations to the Deanship of Scientific Research at King Saud University for its funding this Prolific Research group (PRG-1436-26).

ORCID

Anees A. Ansari http://orcid.org/0000-0002-8708-6673

References

[1] Yen H, Seo Y, Kaliaguine S, et al. Tailored mesostructured copper/ceria catalysts with enhanced performance for preferential oxidation of CO at low temperature. Angew Chem Int Ed. 2012;51:12032−12035.
[2] Mahammadunnisa S, Reddy PMK, Lingaiah N, et al. NiO/$Ce_{1-x}Ni_xO_{2-\delta}$ as an alternative to noble metal catalysts for CO oxidation. Catal Sci Technol. 2013;3:730−737.
[3] Banerjee S, Devi PS, Topwal D, et al. Enhanced ionic conductivity in $Ce_{0.8}Sm_{0.2}O_{1.9}$: unique effect of calcium co-doping. Adv Funct Mater. 2007;17:2847−2854.
[4] Robert CL, Long JW, Pettigrew KA, et al. Ionic nanowires at 600°C: using nanoarchitecture to optimize electrical transport in nanocrystalline gadolinium-doped ceria. Adv Mater. 2007;19:1734−1739.
[5] Yu T, Zeng J, Lim B, et al. Aqueous-phase synthesis of Pt/CeO_2 hybrid nanostructures and their catalytic properties. Adv Mater. 2010;22:5188−5192.
[6] Liao L, Mai HX, Yuan Q, et al. Single CeO_2 nanowire gas sensor supported with Pt nanocrystals: gas sensitivity, surface bond states, and chemical mechanism. J Phys Chem C. 2008;112:9061−9065.
[7] Si R, Zhang YW, You LP, et al. Rare-earth oxide nanopolyhedra, nanoplates, and nanodisks. Angew Chem Int Ed. 2005;44:3256−3260.
[8] Yu T, Joo J, Park YI, et al. Large-scale nonhydrolytic sol−gel synthesis of uniform-sized ceria nanocrystals with spherical, wire, and tadpole shapes. Angew Chem Int Ed. 2005;44:7411−7414.
[9] Ansari AA, Sumana G, Pandey MK, et al. Sol-gel-derived titanium oxide−cerium oxide biocompatible nanocomposite film for urea sensor. J Mater Res. 2009;24:1667−1674.
[10] Ansari AA, Sumana G, Khan R, et al. Polyaniline-cerium oxide nano-composite for hydrogen peroxide sensor. J Nanosci Nanotech. 2009;9:4679−4686.
[11] Radovic M, Mitrovic ZD, Golubovic A, et al. Influence of Fe^{3+}-doping on optical properties of CeO_{2-y} nanopowders. Ceram Intern. 2013;39:4929−4936.
[12] Wen QY, Zhang HW, Yang QH, et al. Effects of oxygen vacancies on the room-temperature ferromagnetism of Co-doped polycrystalline CeO_2. J Magn. Magn Mater. 2009;321:3110−3113.
[13] Bamwenda GR, Arakawa H. Cerium dioxide as a photocatalyst for water decomposition to O_2 in the presence of Ce_{aq}^{4+} and Fe_{aq}^{3+} species. J Molec Cataly A. 2000;161:105−113.
[14] Zheng X, Zhang X, Fang Z, et al. Characterization and catalysis studies of CuO/CeO_2 model catalysts. Catal Commun. 2006;7:701−704.
[15] Kossoy A, Feldman Y, Wachtel E, et al. Elasticity of solids with a large concentration of point defects II. The chemical strain effect in $Ce_{0.8}Gd_{0.2}O_{1.9}$. Adv Funct Mater. 2007;17:2393−2398.
[16] Fu Q, Deng W, Saltsburg H, et al. Activity and stability of low-content gold−cerium oxide catalysts for the water−gas shift reaction. Appl Catal B. 2005;56:57−68.
[17] Chang S, Li M, Hua Q, Zhang L, et al. Shape-dependent interplay between oxygen vacancies and Ag−CeO_2 interaction in Ag/CeO_2 catalysts and their influence on the catalytic activity. J Catalysis. 2012;293:195−204.
[18] Chen PL, Chen IW. Grain growth in CeO_2: dopant effects, defect mechanism, and solute drag. J Am Ceram Soc. 1996;79:1793−1800.
[19] Kumar S, Gautam S, Song TK, et al. Electronic structure study of Co doped CeO_2 nanoparticles using X-ray absorption fine structure spectroscopy. J Alloys Comp. 2014;611:329−334.
[20] Zhang T, Hing P, Huang H, et al. Sintering and grain growth of CoO-doped CeO_2 ceramics. J Eur Ceramic Soc. 2002;22:27−34.
[21] Wen QY, Zhang HW, Yang QH, et al. Effects of oxygen vacancies on the room-temperature ferromagnetism of Co-doped polycrystalline CeO_2. J Magn Magn Mater. 2009;321:3110−3113.
[22] Varela JA, Cerri JA, Leite ER, et al. Microstructural evolution during sintering of CoO doped SnO_2 ceramics. Ceram Inter. 1999;25:253−256.

[23] Cerri JA, Leite ER, Gouvea D, et al. Effect of cobalt(II) oxide and manganese(IV) oxide on sintering of tin(IV) oxide. J Am Ceram Soc. 1996;79:799−804.
[24] Wang Z, Quan Z, Lin J. Remarkable changes in the optical properties of CeO_2 nanocrystals induced by lanthanide ions doping. Inorg Chem. 2007;46:5237−5244.
[25] Babu S. Schulte A, Seal S. Defects and symmetry influence on visible emission of Eu doped nanoceria. Appl Phys Lett. 2008;92:123112−123113.
[26] Mitrovic ZDD, Radovic M, Scepanovic M, et al. Temperature-dependent Raman study of $Ce_{0.75}Nd_{0.25}O_{2-\delta}$ nanocrystals. Appl Phys Lett. 2007;91:203118.
[27] Zhang J, Guo J, Liu W, et al. Facile preparation of M*n*+-doped (M = Cu, Co, Ni, Mn) hierarchically mesoporous CeO_2 nanoparticles with enhanced catalytic activity for CO oxidation. Eur J Inorg Chem. 2015;969−977.
[28] Ansari AA, Singh SP, Malhotra BD. Optical and structural properties of nanostructured CeO_2: Tb^{3+} film. J Alloy Comp. 2011;509:262−265.
[29] Li HF, Lu GZ, Wang YQ, et al. Synthesis of flower-like La or Pr-doped mesoporous ceria microspheres and their catalytic activities for methane combustion. Catal Commun. 2010;11:946−950.
[30] Thurber A, Reddy KM, Shutthanandan V, et al. Ferromagnetism in chemically synthesized CeO_2 nanoparticles by Ni doping. Phys Rev B. 2007;76:165206−165203.
[31] Wen QY, Zhang HW, Song YQ, et al. Room-temperature ferromagnetism in pure and Co doped CeO_2 powders. J Phys. 2007;19:246205−246207.
[32] Ou YN, Li GR, Liang JH, et al. $Ce_{1-x}Co_xO_{2-\delta}$ nanorods grown by electrochemical deposition and their magnetic properties. J Phys Chem C. 2010;114:13509−13514.
[33] Phokha S, Pinitsoontorn S, Maensiri S. Structure and magnetic properties of monodisperse Fe^{3+}-doped CeO_2 nanospheres. Nano-Micro Lett. 2013;5:223−233.
[34] Ansari AA, Kaushik A. Synthesis and optical properties of nanostructured Ce(OH). J Semicond. 2010;31:033001−033004.
[35] Ansari AA, Kaushik A, Solanki PR, et al. Sol−gel derived nanoporous cerium oxide film for application to cholesterol biosensor. Electrochem Commun. 2008;10:1246−1249.
[36] Ansari AA. Optical and structural properties of sol-gel derived nanostructured CeO_2 film. J. Semicond. 2010;31:053001−053005.
[37] Khan MA, Woo SI, Yang OB. Hydrothermally stabilized Fe(III) doped titania active under visible light for water splitting reaction. Intern J Hydrogen Energy. 2008;33:5345−5351.
[38] Miao JJ, Wang H, Li YR, et al. Ultrasonic-induced synthesis of CeO_2 nanotubes. J Crys Growth. 2005;281:525−529.
[39] Saranya J, Ranjith KS, Saravanan P, et al. Cobalt-doped cerium oxide nanoparticles: enhanced photocatalytic activity under UV and visible light irradiation. Mater Sc Semicond Process. 2014;26:218−224.
[40] Yue L, Zhang XM. Structural characterization and photocatalytic behaviors of doped CeO_2 nanoparticles. J Alloys Comp. 2009;475:702−705.
[41] Masui T, Fujiwara K, Machida K, et al. Characterization of cerium(IV) oxide ultrafine particles prepared using reversed micelles. Chem Mater. 1997;9:2197−2204.
[42] Patsalas P, Logothetidis S, Sygelloou L, et al. Structure-dependent electronic properties of nanocrystalline cerium oxide films. Phys Rev B. 2003;68:035104.
[43] Luo JY, Meng M, Yao JS, et al. One-step synthesis of nanostructured Pd-doped mixed oxides MO_x-CeO_2 (M = Mn, Fe, Co, Ni, Cu) for efficient CO and C_3H_8 total oxidation. Appl Cataly B. 2009;87:92−103.
[44] Zhang F, Chen CH, Raitano JM, et al. Phase stability in ceria-zirconia binary oxide nanoparticles: The effect of the Ce^{3+} concentration and the redox environment. J Appl Phys. 2006;99:084313−084318.
[45] Cunni X, Shaofei W, Chunwen S, et al. Effect of Ni doping on the catalytic properties of nanostructured peony-like CeO_2. Chin J Catalysis. 2013;34:305−312.
[46] Zhang D, Qian Y, Shi L, et al. Cu-doped CeO_2 spheres: synthesis, characterization, and catalytic activity. Cataly Commun. 2012;26:164−168.